



Analysis of Temperature-Dependent Photoluminescence Spectra in Mid-Wavelength Infrared InAs/InAsSb Type-II Superlattice

K. Murawski¹ · T. Manyk¹ · M. Kopytko¹

Received: 6 January 2023 / Accepted: 31 July 2023
© The Author(s) 2023

Abstract

Photoluminescence (PL) is one of the commonly used methods to determine the energy gap (E_g) of semiconductors. In order to use it correctly, however, the shape of the PL peak must be properly analyzed; otherwise, the value of E_g is burdened with a large error. E_g is often mistakenly attributed to the PL peak position, which in type-II superlattices (T2SLs) exhibits typical “S-shaped” behavior as a function of temperature, significantly different from the Varshni model used to define the energy gap of III-V compounds. The position peak of the PL relative to the real E_g in T2SLs is red-shifted because of the carrier localization at low temperatures and blue-shifted because of the free carrier emission at high temperatures. To correctly determine E_g , the shape of the PL peak should be analyzed using the theoretical PL line shape model that takes into account both localized (below the bandgap) and free carriers (above the bandgap) emissions. This work shows that the use of such a model to analyze the shape of the PL signal gives the correct results of determining E_g for mid-wave infrared InAs/InAsSb T2SL, which showed a significant contribution of localized states in optical transitions and characteristic “S-shaped” PL peak behavior. This allowed us to determine the correct values of the Varshni coefficients for a given T2SL. The result also agrees with the theoretical calculations of E_g made using the k-p method.

Keywords Type-II superlattices · photoluminescence spectroscopy · carrier localization · infrared detectors · “S-shaped” PL peak behavior

Introduction

The interest in the fabrication and study of Ga-free InAs/InAsSb type-II superlattices (T2SLs) is related to their potential to replace HgCdTe in infrared (IR) detector technology. Recently demonstrated photodetectors with nBn— or more generally XBn—design offer many advantages in realizing high-performance devices.^{1–3} The wide-bandgap barrier layer, which is located between the cap contact and the absorber, blocks the flow of majority carriers (electrons) in the conduction band but allows the flow of minority carriers (holes) in the valence band. This architecture offers the benefits of reduced dark current due to the suppression of

the Shockley–Read–Hall (SRH) recombination process over conventional III-V-based p – n junction photodiodes.

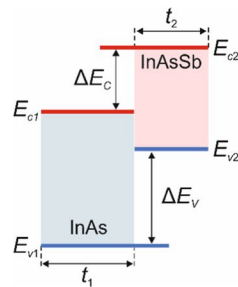
A proper band alignment between the barrier and the absorber is the key issue in designing such a structure. Otherwise, undesirable barriers are formed in the valence band that inhibit the flow of minority carrier holes from the absorber to the contact.^{4,5} Then, a relatively high bias needs to be applied to the device in order to improve photogenerated carrier collection efficiency. Thus, the correct design of the nBn detector requires knowledge of energy gaps of the materials and the mutual positioning of the bands between them.

The effective energy gap (E_g) of InAs/InAsSb T2SL is determined by the energy difference between the lowest electron mini-band (C1) and the highest hole mini-band (HH1) in the center of the Brillouin zone (see Fig. 1). Electrons are confined in the InAs layer, whereas the holes are confined to the InAsSb layer; therefore, the transition occurs only where the probability distribution functions overlap. The position of mini-bands depends on (1) the thickness of

✉ M. Kopytko
malgorzata.kopytko@wat.edu.pl

¹ Institute of Applied Physics, Military University of Technology, 2 Kaliskiego St., 00-908 Warsaw, Poland

Fig. 1 Bandgap diagram for InAs/InAsSb T2SLs.



the component layers, (2) the composition of the InAsSb layer, and (3) the band offset of individual layers, which is also influenced by the bandgap bowing in the InAsSb alloy.

The temperature dependence of the InAs/InAsSb T2SL, similarly to all III-V group semiconductors, can be approximated by the Varshni equation:⁸

$$E_g(T) = E_0 - \frac{\alpha T^2}{T + \beta}, \quad (1)$$

where E_0 is the bandgap at 0 K, and α and β are the Varshni coefficients.

However, the experimental determination of E_g and its temperature dependence is not a simple task for InAs/InAsSb T2SL. One of the most common methods used to determine E_g is photoluminescence (PL). In T2SLs, the position peak of the PL exhibits typical “S-shaped” behavior as a function of temperature,^{6,7} significantly different from the Varshni relation.⁸ Similar “S-shaped” behavior is also observed in nitrogen- and aluminum-containing semiconductors,^{9–15} and is related to the carrier localization phenomenon.^{9,10,13}

Compositional variation, layer width fluctuations, and/or high density of impurities or dopants lead to the formation of local states past the band edges, which in disordered semiconductors are distributed randomly. At low temperatures, mainly deep localization centers are filled with carriers, and the observed PL is mainly due to the transition between these centers (Fig. 2a). The PL peak might be fitted using a theoretical model which assumes the Gaussian density of localized states,¹⁶ and then shows a red shift in relation to E_g .

The rise in temperature enables the filling of shallow localization centers, thus shifting the emission peak towards the band edges. At high temperatures, free carrier emission—the transition of free electrons from the conduction band (CB) to the valence band (VB)—becomes dominant in the PL signal (Fig. 2b). The shape of the PL signal is asymmetric: the high-energy side of the PL peak related to the Fermi–Dirac (F–D) carrier distribution function is broadened, while the low-energy side of the PL peak is sharp. The band edge is defined by the density of states (DOS) function—the PL peak energy is blue-shifted in relation to E_g . The decreasing below-band-edge emission can be described by the Urbach tail.

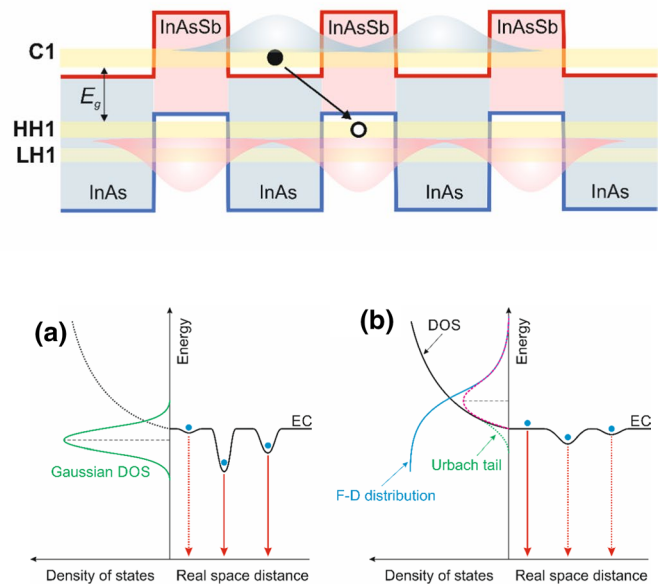


Fig. 2 Schematic diagram of energy vs. density of states and real spatial distribution: (a) transitions from localized states dominate at low temperatures. The PL signal is described by the Gaussian density of localized states—the PL peak energy is red-shifted in relation to E_g ; and (b) transition of free electrons dominates at high temperatures. The PL signal is described by the product of the Fermi–Dirac (F–D) carrier distribution function and the density of states (DOS) function—the PL peak energy is blue-shifted in relation to E_g . EC is the conduction band edge.

In our analysis, we determine the energy gap of the InAs/InAsSb T2SL using a functional form of the PL line shape model, $I_{PL}(E)$, described next. It gave a good agreement with the theoretical calculations of E_g made using the k-p method and allows for the correct determination of Varshni coefficients for a temperature-dependent energy gap.

Photoluminescence Shape Model

PL is the emission of light from a semiconductor sample after excitation by a laser. The emission spectrum is created by exciting electrons at a fixed wavelength but observing emissions at different wavelengths. Intrinsic (band-to-band) PL originates from radiative transitions of excited electrons in the CB to empty states in the VB. Then, the PL spectrum emitted from the sample can be described by the product of the DOS and the probability that the particle occupies a state with the energy E —the above-band-edge emission. However, the real material systems always incorporate impurities or structural disorders which can lead to the localization of carriers. Thus, we have used the following PL line shape model, which additionally incorporates an Urbach tail for the below-band-edge emission^{9,17–19}:

$$I_{\text{PL}}(E > E_{\text{cr}}) = A(E - E_{\text{g}})^n \times \left[1 + \exp\left(\frac{E - E_{\text{g}}}{k_{\text{B}}T}\right) \right]^{-1}, \quad (2)$$

$$I_{\text{PL}}(E \leq E_{\text{cr}}) = AK \exp\left[\frac{2\sigma n}{k_{\text{B}}T}(E - E_{\text{cr}})\right] \times \left[1 + \exp\left(\frac{E - E_{\text{g}}}{k_{\text{B}}T}\right) \right]^{-1}, \quad (3)$$

where E_{cr} is the energy of transition (or crossover) between Eqs. 2 and 3, E_{g} is the bandgap energy, T is temperature, k_{B} is the Boltzmann constant, K is a dummy parameter chosen to ensure that the transition is a smooth one, σ is a dimensionless phenomenological parameter describing the slope of the Urbach tail, and A is related to the Einstein coefficient linking the conduction and valence band states (but is treated here as a fitting parameter). The continuity and smoothness of the function given by Eqs. 2 and 3 is ensured when $E_{\text{cr}} = E_{\text{g}} + k_{\text{B}}T/2\sigma$ and $K = (k_{\text{B}}T/2\sigma)^n$. The n parameter can vary from 0.5 for conserved momentum to 2 for non-conserved momentum inter-band transitions. We have assumed that the F–D carrier distribution function is appropriate for the electron and hole occupations. Applying the Boltzmann statistic would lead to an overestimation of the value of the energy gap.¹⁹

Results

The experimental data used in the analysis were extracted from the paper of Steenberg et al.⁶ InAs(6.7 nm)/InAs_{0.66}Sb_{0.34}(1.8 nm) T2SL was grown by molecular beam epitaxy (MBE) at IQE Inc. on an undoped GaSb substrate. The PL spectra of the sample showed a significant contribution of localized states in optical transitions and characteristic S-shaped behavior of the PL peak energy. For the results described by Steenberg et al.,⁶ the PL signal was measured with a 12- μm cutoff HgCdTe detector. A 532-nm laser modulated with a frequency of 60 Hz was used as an excitation source. The measurement was made under low excitation conditions (1.5 W/cm²).

To investigate the nature of the emission from InAs(6.7 nm)/InAs_{0.66}Sb_{0.34}(1.8 nm) T2SL, the PL spectra at different temperatures were examined (Fig. 3). From 25 K to 240 K, the PL signal was fitted with the $I_{\text{PL}}(E)$ model, which is a combination of Eqs. 2 and 3. In the temperature range from 120 K to 240 K, the PL signal shows an asymmetric shape. A significant contribution of a free carrier emission causes a broadening of the high-energy side of the PL peak. The decreasing below-band-edge emission can be described by the Urbach tail. A small proportion of localized states causes a sharp slope of the Urbach tail at the low-energy side of the PL peak. With decreasing temperature, the high-energy slope becomes

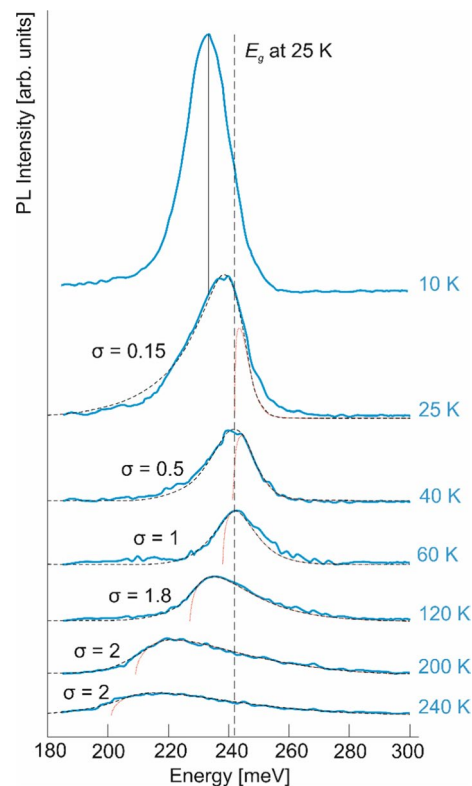


Fig. 3 Temperature-dependent PL spectra for InAs(6.7 nm)/InAs_{0.66}Sb_{0.34} (1.8 nm) T2SL. The experimental data were extracted from the paper of Steenberg et al.⁴ The dark dotted line represents the best fit to the PL peak using the $I_{\text{PL}}(E)$ line shape model. For each temperature, the σ parameter associated with the participation of the Urbach tail was determined. The red dotted line represents a fit to the PL peak using Eq. 2. The intersection with the abscissa allows us to determine the energy gap. The vertical dashed line represents E_{g} at 25 K (Color figure online).

sharper due to the narrowing of the F–D function. Broadening of the low-energy slope at low temperatures indicates band tails in the joint density of states, which are due to localized states past the band edges. As the peak broadens, the σ parameter describing the slope of the Urbach tail at the low-energy side of the PL peak decreases. The latter may contribute in particular at very low temperatures, where the PL signal has a Gaussian-like shape and the PL peak is located much lower than the energy gap. At 10 K, transitions through deep localized states dominate, and it is difficult to determine E_{g} by fitting the $I_{\text{PL}}(E)$ model.

Figure 4 shows the PL peak position and the bandgap energy as a function of temperature. The blue dotted line is a fit to the PL peak position, while the black dotted line is a fit of the Varshni equation to E_{g} . At temperatures above 40 K, the PL peak is blue-shifted in relation to E_{g} . The PL peak position overestimates the effective E_{g} by a value close to $k_{\text{B}}T$. At temperatures below 40 K, in turn, the PL peak position is red-shifted because of the carrier localization. At

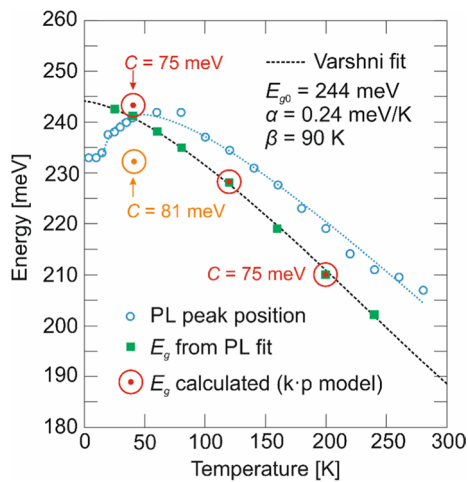


Fig. 4 PL peak position (blue open circles) and the bandgap energy (green squares) vs. temperature for InAs(6.7 nm)/InAs_{0.66}Sb_{0.34}(1.8 nm) T2SL. The blue dotted line is a fit to the PL peak position, and the black dotted line is a fit of the Varshni equation to E_g . The red circles show the theoretical energy gap calculated using the k·p model for different InAsSb energy gap bowing (Color figure online).

Table I Parameters of the binary InAs and ternary InAs_{0.66}Sb_{0.34} materials at $T=200$ K

Parameter	InAs	InAs _{0.66} Sb _{0.34}
E_g (meV)	379	178
Δ_{SO} (meV)	390	264
m_e/m_0	0.0237	0.0115
γ_1	20.00	42.544
γ_2	8.50	19.598
γ_3	9.20	20.426

10 K, the PL peak is located at around 10 meV below the bandgap due to a high density of localized states.

It is worth noting that the determined E_g agrees with theoretical values (red circles) calculated for the given superlattice. Calculations were made with a commercially available APSYS platform (Crosslight Inc.),²⁰ which is based on the four-band (8×8 Hamiltonian) k-p model. The position of the mini-bands (C1 and HH1) and the absorption spectrum were determined from knowledge of the thickness of the InAs and InAsSb in each superlattice period. The main input data for T2SL modeling are shown in Table I. The Luttinger parameters ($\gamma_1, \gamma_2, \gamma_3$) were estimated based on the respective effective masses (m_{lh}, m_{hh}, m_{SO}).²¹

The schematic representation of the energy bands of the strained InAs(6.7 nm)/InAs_{0.66}Sb_{0.34}(1.8 nm) T2SL at 200 K is presented in Fig. 5. The figure also shows the C1 and HH1 mini-band edges and the probability distribution functions for electrons and heavy holes. The periodic boundary conditions were used in the simulation procedure, which

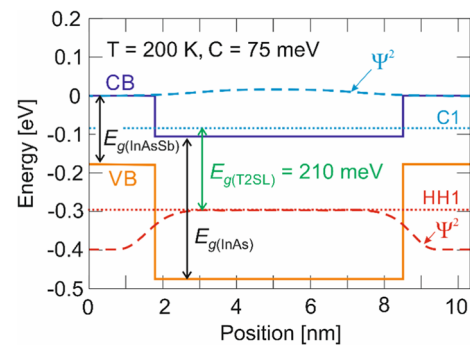


Fig. 5 Calculated band structure of InAs(6.7 nm)/InAs_{0.66}Sb_{0.34}(1.8 nm) T2SL structure with periodic boundary conditions at 200 K (CB—conduction band, VB—valence band, C1—first electron mini-band, HH1—first heavy hole mini-band, E_g —bandgap energy, and Ψ^2 —probability distribution functions).

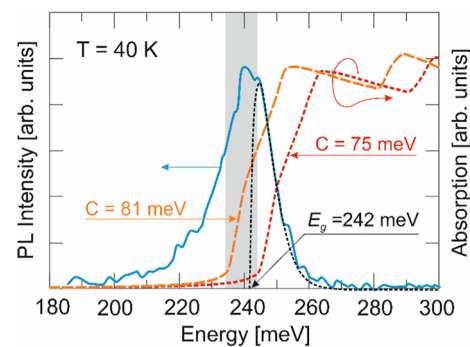


Fig. 6 Calculated absorption (red and orange dashed lines) and measured PL spectra (blue solid line) for InAs(6.7 nm)/InAs_{0.66}Sb_{0.34}(1.8 nm) T2SL structure at 40 K. Absorption was calculated for the wave vector of $k=0.01$ ($2\pi/a$) and two energy gap bowing parameter values: $C=75$ meV (red dashed line) and $C=81$ meV (orange dashed line). The dark dotted line represents the best fit to the PL peak using the model described by Eq. 2 (Color figure online).

impose periodicity on the wave functions. The experimental E_g is consistent with the calculated value of 210 meV for an assumed bowing parameter of $C=75$ meV.

At low temperatures, however, the calculated E_g differs from the experimental one (see Fig. 4). This is because the InAsSb bandgap bowing parameter is not constant, but changes with temperature. Webster et al.²² determined the temperature-dependent bowing parameter. They estimated low-temperature and room-temperature bandgap bowing of $C=938$ meV at 0 K and $C=750$ meV at 295 K.

Figure 6 compares the simulated absorption spectra for two values of the InAsSb energy gap bowing parameter with the measured PL spectra of the InAs(6.7 nm)/InAs_{0.66}Sb_{0.34}(1.8 nm) T2SL at 40 K. The calculated energy gap, depending on the bowing, ranges from 234 meV (for $C=81$ meV) to 244 meV (for $C=75$ meV). The energy gap was determined by the best fit to the PL peak using the

model described by Eq. 2, and is between the calculated values for two bowing parameters. This suggests that the InAsSb energy gap bowing parameter increases slightly with decreasing temperature, which was also confirmed by other theoretical calculations.^{23,24}

Conclusions

Since the PL from the InAs/InAsSb layers contains a significant contribution of localized emission at low temperatures and free carrier emission at high temperatures, the temperature dependence of the PL peak position shows “S-shaped” behavior, significantly different from the Varshni model for the energy gap. By taking the theoretical dependence as a product of the joint density of states and the F–D distribution function, which additionally incorporates an Urbach tail for the below-band-edge emission, we are able to determine the effective energy gap relationship for T2SL. The Varshni parameters determined for the bandgap extracted from the PL spectra by the fitting procedure are very similar to those observed in InAs and InAsSb. The model gives results comparable to the value of the energy gap obtained from theoretical calculations made using the k-p method.

Funding This study was funded by the National Centre for Research and Development (Poland) under Grant POIR.01.01.01-00-0185/20-00.

Conflict of interest The authors declare that they have no conflict of interest.

Open Access This article is licensed under a Creative Commons Attribution 4.0 International License, which permits use, sharing, adaptation, distribution and reproduction in any medium or format, as long as you give appropriate credit to the original author(s) and the source, provide a link to the Creative Commons licence, and indicate if changes were made. The images or other third party material in this article are included in the article's Creative Commons licence, unless indicated otherwise in a credit line to the material. If material is not included in the article's Creative Commons licence and your intended use is not permitted by statutory regulation or exceeds the permitted use, you will need to obtain permission directly from the copyright holder. To view a copy of this licence, visit <http://creativecommons.org/licenses/by/4.0/>.

References

1. D.Z.-Y. Ting, A. Soibel, S.A. Keo, A. Khoshakhlagh, C.J. Hill, L. Höglund, J.M. Mumolo, and S.D. Gunapala, Superlattice and Quantum Dot Unipolar Barrier Infrared Detectors. *J. Electron. Mater.* 42(11), 3071–3079 (2013). <https://doi.org/10.1007/s11664-013-2641-9>.
2. A. Soibel, D.Z. Ting, S.B. Rafol, A.M. Fisher, S.A. Keo, A. Khoshakhlagh, and S.D. Gunapala, Mid-wavelength Infrared InAsSb/InAs nBn Detectors and FPAs with Very Low Dark Current Density. *Appl. Phys. Lett.* 114(16), 161103 (2019). <https://doi.org/10.1063/1.5092342>.
3. P.C. Klipstein, Y. Gross, D. Aronov, and M. ben Ezra, E. Berkowicz, Y. Cohen, R. Fraenkel, A. Glozman, S. Grossman, O. Klin, I. Lukomsky, T. Marlowitz, L. Shkedy, I. Shtrichman, N. Snapi, A. Tuito, M. Yassen, and E. Weiss, Low SWaP MWIR Detector Based on XBn Focal Plane Array. *Proc. SPIE* 8704, 87041S (2013). <https://doi.org/10.1117/12.2015747>.
4. S. Maimon, and G.W. Wicks, nBn Detector, An Infrared Detector with Reduced Dark Current and Higher Operating Temperature. *Appl. Phys. Lett.* 89(15), 151109 (2006). <https://doi.org/10.1063/1.2360235>.
5. J.B. Rodriguez, E. Plis, G. Bishop, Y.D. Sharma, H. Kim, L.R. Dawson, and S. Krishna, nBn Structure Based on InAs/GaSb Type-II Strained Layer Superlattices. *Appl. Phys. Lett.* 91, 043514-1–43522 (2007). <https://doi.org/10.1063/1.2760153>.
6. E.H. Steenbergen, J.A. Massengale, G. Ariyawansa, and Y.H. Zhang, Evidence of Carrier Localization in Photoluminescence Spectroscopy Studies of Mid-wavelength Infrared InAs/InAs_{1-x}Sb_x type-II Superlattices. *J. Lumin.* 178, 451–456 (2016). <https://doi.org/10.1016/j.jlumin.2016.06.020>.
7. A. Soibel, D.Z. Ting, C.J. Hill, A.M. Fisher, L. Höglund, S.A. Keo, and S.D. Gunapala, Extended Cut-Off Wavelength nBn Detector Utilizing InAsSb/InSb Digital Alloy Absorber. *Proc. SPIE* 1, 10111 (2017). <https://doi.org/10.1117/12.2251703>.
8. Y.P. Varshni, Temperature Dependence of the Energy Gap in Semiconductors. *Physica* 34, 149–154 (1967). [https://doi.org/10.1016/0031-8914\(67\)90062-6](https://doi.org/10.1016/0031-8914(67)90062-6).
9. M. Latkowska, R. Kudrawiec, F. Janiak, M. Motyka, J. Misiewicz, Q. Zhuang, A. Krier, and W. Walukiewicz, Temperature Dependence of Photoluminescence from InNAsSb Layers: The Role of Localized and Free Carrier Emission in Determination of Temperature Dependence of Energy Gap. *Appl. Phys. Lett.* 102(12), 122109 (2013). <https://doi.org/10.1063/1.4798590>.
10. L. Grenouillet, C. Bru-Chevallier, G. Guillot, P. Gilet, P. Duvaut, C. Vannuffel, A. Million, and A. Chenevas-Paule, Evidence of Strong Carrier Localization Below 100 K in a GaInNAs/GaAs Single Quantum Well. *Appl. Phys. Lett.* 76(16), 2241–2243 (2000). <https://doi.org/10.1063/1.126308>.
11. S.A. Lourenc, I.F.L. Dias, J.L. Duarte, E. Laureto, V.M. Aquino, and J.C. Harmand, Temperature-Dependent Photoluminescence Spectra of GaAsSb/AlGaAs and GaAsSbN/GaAs Single Quantum Wells under Different Excitation Intensities. *Braz. J. Phys.* 37(4), 1212–1219 (2007). <https://doi.org/10.1590/S0103-97332007000800004>.
12. P.A. Drózd, K.P. Korona, M. Sarzynski, R. Czernecki, C. Skierbiszewski, G. Muzioł, and T. Suski, A Model of Radiative Recombination in (In, Al, Ga)N/GaN Structures with Significant Potential Fluctuations. *Acta Phys. Pol. A* 130(5), 1209–1212 (2016). <https://doi.org/10.12693/APhysPolA.130.1209>.
13. N.V. Kryzhanovskaya, A.G. Gladyshev, D.S. Sizov, A.R. Kovsh, and A.F. Tsatsul'nikov, J.Y. Chi, J.-S. Wang, L.-C. Wei, V.M. Ustinov, The carriers localization influence on the optical properties of GaAsN/GaAs heterostructures grown by molecular-beam epitaxy. *Proc. SPIE* 5023, 1 (2003). <https://doi.org/10.1117/12.510522>.
14. T. Yamamoto, M. Kasu, S. Noda, and A. Sasaki, Photoluminescent Properties and Optical Absorption of AlAs/GaAs Disordered Superlattices. *J. Appl. Phys.* 68(10), 5318–5323 (1990). <https://doi.org/10.1063/1.347025>.
15. M. Kasu, T. Yamamoto, S. Noda, and A. Sasaki, Photoluminescent Properties of AlAs/Al_xGa_{1-x}As (x=0.5) Disordered Superlattices. *Jpn. J. Appl. Phys.* 29, L1055–L1058 (1990). <https://doi.org/10.1143/JJAP.29.L1055>.
16. P.G. Eliseev, The Red $\sigma_2/kT\sigma_2/kT$ Spectral Shift in Partially Disordered Semiconductors. *J. Appl. Phys.* 93(9), 5404–5415 (2003). <https://doi.org/10.1063/1.1567055>.

17. K. Murawski, M. Kopytko, P. Madejczyk, K. Majkowycz, and P. Martyniuk, HgCdTe Energy Gap Determination from Photoluminescence and Spectral Response Measurements. *Metrol. Meas. Syst.* 30(1), 183–194 (2023). <https://doi.org/10.24425/mms.2023.144395>.
18. Z.M. Fang, K.Y. Ma, D.H. Jaw, R.M. Cohen, and G.B. Stringfellow, Photoluminescence of InSb, InAs, and InAsSb Grown by Organometallic Vapor Phase Epitaxy. *J. Appl. Phys.* 67(11), 7034–7039 (1990). <https://doi.org/10.1063/1.345050>.
19. M. Merrick, S.A. Cripps, B.N. Murdin, T.J.C. Hosea, T.D. Veal, C.F. McConville, and M. Hopkinson, Photoluminescence of InNAs Alloys: S-Shaped Temperature Dependence and Conduction-Band Nonparabolicity. *Phys. Rev. B* 76, 075209 (2007). <https://doi.org/10.1103/PhysRevB.76.075209>.
20. Crosslight Device Simulation Software—General Manual 2019 version. Crosslight Software Inc. (2019). <https://crosslight.com/>
21. M. Ehrhardt, and T. Koprucki, *Multi-Band Effective Mass Approximations*. In: *Advanced Mathematical Models and Numerical Techniques* (Cham: Springer, 2014).
22. P.T. Webster, N.A. Riordan, S. Liu, E.H. Steenbergen, R.A. Synowicki, Y.H. Zhang, and S.R. Johnson, Measurement of InAsSb Bandgap Energy and InAs/InAsSb Band Edge Positions Using Spectroscopic Ellipsometry and Photoluminescence Spectroscopy. *J. Appl. Phys.* 118(24), 245706 (2015). <https://doi.org/10.1063/1.4939293>.
23. T. Manyk, K. Michalczewski, K. Murawski, K. Grodecki, J. Rutkowski, and P. Martyniuk, Electronic Band Structure of InAs/InAsSb Type-II Superlattice for HOT LWIR Detectors. *Res. Phys.* 11, 1119–1123 (2018). <https://doi.org/10.1016/j.rinp.2018.11.030>.
24. T. Manyk, K. Michalczewski, K. Murawski, P. Martyniuk, and J. Rutkowski, InAs/InAsSb Strain-Balanced Superlattices for Long-wave Infrared Detectors. *Sensors* 19, 1907 (2019). <https://doi.org/10.3390/s19081907>.

Publisher's Note Springer Nature remains neutral with regard to jurisdictional claims in published maps and institutional affiliations.